Refined measurement of SecA-driven protein secretion reveals that translocation is indirectly coupled to ATP turnover

William J. Allen[a], Daniel W. Watkins[a], Mark S. Dillingham[a], and Ian Collinson[a,1]

[a]School of Biochemistry, University of Bristol, BS8 1TD Bristol, United Kingdom

Edited by Randy Schekman, University of California, Berkeley, CA, and approved October 29, 2020 (received for review May 29, 2020)

The universally conserved Sec system is the primary method cells utilize to transport proteins across membranes. Until recently, measuring the activity—a prerequisite for understanding how biological systems work—has been limited to discontinuous protein transport assays with poor time resolution or reported by large, nonnatural tags that perturb the process. The development of an assay based on a split superbright luciferase (NanoLuc) changed this. Here, we exploit this technology to unpick the steps that constitute posttranslational protein transport in bacteria. Under the conditions deployed, the transport of a model preprotein substrate (proSpy) occurs at 200 amino acids (aa) per minute, with SecA able to dissociate and rebind during transport. Prior to that, there is no evidence for a distinct, rate-limiting initiation event. Kinetic modeling suggests that SecA-driven transport activity is best described by a series of large (~30 aa) steps, each coupled to hundreds of ATP hydrolysis events. The features we describe are consistent with a nondeterministic motor mechanism, such as a Brownian ratchet.

protein secretion | molecular motor | NanoLuc | SecYEG | SecA

To transport proteins from one side of a lipid bilayer to the other, cells employ specialized, membrane-embedded molecular motors. These recognize proteins for transport and then use energy from ATP binding and hydrolysis and/or the protonmotive force (PMF) to transfer them through a polypeptide-conducting channel in the membrane—usually threading them through in an unfolded state. Probably the best-studied protein transporter is the *Escherichia coli* version of the ubiquitous Sec system, which handles almost all proteins destined for the cell envelope and beyond. In its posttranslational mode—used for exporting periplasmic, outer-membrane, and extracellular proteins—the cytosolic ATPase SecA binds preproteins with a cleavable N-terminal signal sequence (SS) and translocates them through the membrane-embedded heterotrimeric core-complex SecYEG.

In many ways, the bacterial Sec system is quite well characterized: several structures of the channel complex and motor ATPase SecA are available, alone and associated (1–3); the pathway the preprotein takes and how various domains move have been mapped extensively using biochemical, biophysical, and computational approaches (4–8); and the ATPase activity of SecA and its regulation have been subject to detailed dissection (9–13). Yet despite this, there is no definitive answer to the question, how is ATP hydrolysis actually coupled to protein transport?

Perhaps the biggest barrier to elucidating the mechanism of the Sec machinery is the huge variability of the substrate: a polypeptide composed of sequences of amino acids (aa) of different size, shape, and chemistry. Unlike motors that run along DNA or RNA—which have a repeating sugar-phosphate backbone to grip onto—or those that move along predictably organized cytoskeletal helical filaments, protein transporters must by turns recognize hydrophobic and hydrophilic regions, small and bulky residues with both positive and negative charge, and varying amounts of secondary structure. Thus, no single set of domain movements is likely to work for every part of every preprotein. Instead, current models for Sec are not purely deterministic; they allow at least some measure of preprotein diffusion through the channel. We have previously proposed a pure ratcheted diffusion model (6, 9, 14), while others have proposed a hybrid "push and slide" model, in which ATP-driven power strokes are complemented by an element of diffusion (15).

Very precise measurements of protein transport are required to distinguish between these types of mechanisms, such as those produced by the recently published NanoLuc transport assay (16). Here, we extend the use of the NanoLuc assay to reveal the elementary steps of the ATP-driven protein transport mechanism, using the model preprotein prospheroplast protein Y (pSpy). The results reveal a nondeterministic transport model with a small apparent number of steps, each of which requires hundreds of ATP turnovers in vitro. Transport occurs at an overall rate of about 200 aa per minute, is apparently dependent on the preprotein concentration gradient across the membrane, and is not limited by a distinct initiation step.

Results

Using NanoLuc to Dissect Translocation Kinetics. To interrogate the kinetics of protein transport in sufficient detail to reveal mechanistic information, we used the recently developed NanoLuc system (16). In essence, NanoLuc luciferase missing a single β-strand (11S) is encapsulated within proteoliposomes (PLs) incorporating the Sec machinery, while a high-affinity version of the missing β-strand (Pep86) is fused to a translocation substrate. These are then mixed together in the presence of the luciferase

Significance

The transport of proteins across membranes is fundamental to all life. The biological machinery responsible for this process has been known for some time, but exactly how it works is still contested. In this paper, we describe how a new, high-precision method for measuring protein transport, combined with careful data analysis, can be used to solve this problem. We find that our transport data are best described by a ratchet-type mechanism, in which the protein can diffuse one way but not the other, rather than by physical pushing of the protein.

Author contributions: W.J.A., D.W.W., M.S.D., and I.C. designed research; W.J.A. and D.W.W. performed research; W.J.A., D.W.W., M.S.D., and I.C. analyzed data; and W.J.A., D.W.W., M.S.D., and I.C. wrote the paper.

The authors declare no competing interest.

This article is a PNAS Direct Submission.

[1]To whom correspondence may be addressed. Email: ian.collinson@bristol.ac.uk.

This article contains supporting information online at https://www.pnas.org/lookup/suppl/doi:10.1073/pnas.2010906117/-/DCSupplemental.

First published November 30, 2020.

substrate furimazine and an ATP regeneration system and allowed to equilibrate, and the reaction is started by the addition of ATP. As preprotein is transported into the PLs, Pep86 complements 11S, producing a luminescent signal. This signal is generally proportional to the amount of NanoLuc for the duration of the experiment, although it eventually begins to decay due to furimazine depletion and/or furimamide accumulation. An example import curve, with background subtracted (*SI Appendix*, Fig. S1*A*; 16), is shown in Fig. 1*A*. It can be fitted, as a fairly good approximation, to a simple delay phase (lag) followed by a single exponential with an apparent rate constant (λ) and amplitude (A; Fig. 1*A*).

The observed kinetics are characteristic of "n-step sequential" translocation mechanisms, such as those that have been applied to the analysis of DNA helicase motors (Fig. 1*B*; 17–19), so the lag–exponential fit can be used to extract semiquantitative information from the data. The amplitude (A) corresponds to the amount of NanoLuc that is formed when the reaction reaches completion. The lag before any signal occurs is the result of the accumulation of transport intermediates because translocation of the protein involves multiple consecutive steps with comparable rates (17). It corresponds to the sum of the time constants (i.e., $\sum 1/k_{all}$) for all steps prior to the one that yields the signal (in our case, the final NanoLuc formation step; 19). The λ factor is complex and has a less-obvious physical meaning with respect to the stepping mechanism. It contains information related to rate-limiting steps in the overall pathway as well as both the translocation step size and the static disorder in the stepping rate; we shall return to this point later.

Taking the observed kinetics into account alongside prior knowledge of the sequence of events leading to protein secretion, a minimal reaction scheme for NanoLuc-monitored protein import can be devised for use as an initial framework for analysis (Fig. 1*B*). Firstly, the preprotein substrate must be recognized by the SecYEG–SecA complex (step *i*; on- and off-rates—k_{on} and k_{off}, respectively). Note that in our setup, this step starts at equilibrium, as it does not require any additional input of energy. Recognition is followed by an ATP-dependent initiation step (step *ii*, rate k_{init}), wherein the SS unlocks the channel and primes it for transport (8, 20–23). Transport itself (step *iii*) is driven by a number (n) of ATP-dependent steps, each of which has the rate k_{step}. In a physiological context, these would presumably be assisted by the PMF (24, 25). Finally, once the Pep86 at the C terminus of the protein has been transported into the PL, it must associate with 11S to form mature NanoLuc (step *iv*, with on- and off-rates—k_{onL} and k_{offL}, respectively).

All of these four steps must occur in order for us to measure a transport signal, but this does not necessarily mean they all contribute appreciably to the kinetics. For example, step *ii* is included in the model because there is ample experimental evidence that it is important for recognizing secretory substrates (21, 22), but it might be too fast to affect the shape of the transport curves. Furthermore, even this relatively simple model makes some basic assumptions (e.g., that the initiated complex never dissociates [infinite processivity]), which we discuss below. Note also that because only a tiny quantity of PLs are present in the reaction, the effective concentrations of all components other than SecYEG and 11S remain constant throughout the reaction.

Establishing a Minimal Model for Transport. To explore how the parameters in the above model are related to the observed data, we carried out control experiments related to steps *i* and *iv*. First, we compared reactions initiated by the addition of ATP (Fig. 1*C*, orange line) with those initiated by pSpy–Pep86 or SecA (Fig. 1*C*, purple and green lines, respectively). The only difference between these runs is whether the step (step *i*) is at equilibrium when the reaction starts (ATP) or if the SecYEG–SecA–preprotein complex must form first (SecA or pSpy–Pep86). As the preequilibrated transport reaction (initiated by ATP) has a shorter lag

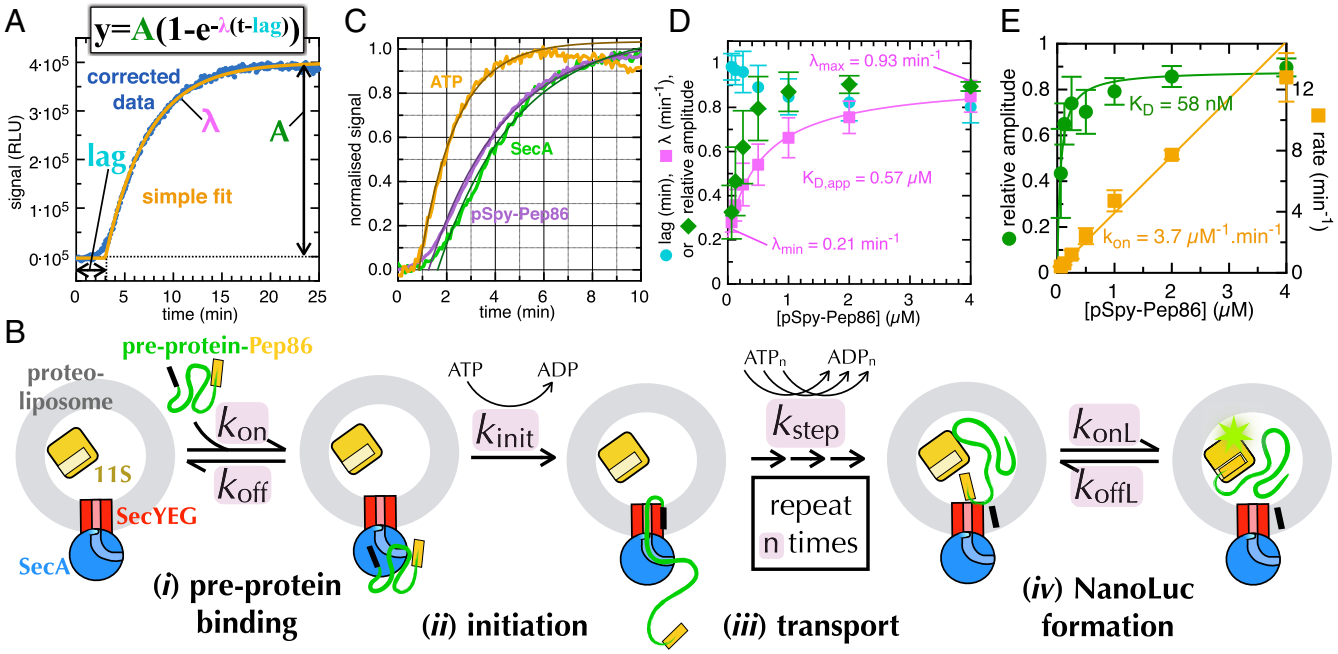

Fig. 1. The NanoLuc transport assay. (*A*) An example NanoLuc transport curve with simple fitting. (*B*) The minimal model used to describe preprotein import in the NanoLuc assay. (*C*) Transport initiated by the addition of ATP (orange), pSpy–Pep86 (purple), or SecA (green). The lines represent best fit to the single exponential plus lag model. (*D*) Fitted λ (pink squares), A (green diamonds), and lag (cyan circles) as a function of pSpy–Pep86 concentration. Error bars represent the average and SEM from four repeats. λ is fitted to a weak binding equation. (*E*) The secondary data from a titration of pSpy–Pep86 against 200 pM 11S in solution. The fits are to a weak binding equation for A (green circles) and a straight line for rate (orange squares).

(lag_{ATP} = 0.85 min) than the two reactions started by the addition of the preprotein or SecA, where step *i* must also take place (lag_{pSpy} = 1.25 min; lag_{SecA} = 1.66 min), at least some transport is occurring from the preformed complex. The difference in lag is equal to k^{-1} of assembly of the preinitiation complex; for 2 μM pSpy, this is 2.5 min^{-1} (1/(1.25 − 0.85)) or 1.25 $\mu M^{-1} \cdot min^{-1}$, while with 1 μM SecA, it is 1.23 min^{-1} (1/(1.66 − 0.85))—also ~1.25 $\mu M^{-1} \cdot min^{-1}$. Because we are most interested in extracting only k_{init}, k_{step}, and n, all subsequent experiments were initiated using ATP.

We next investigated the effect of titrating pSpy–Pep86 concentration on transport. The import signal fits well to the simple exponential + lag fit (example raw data are shown in *SI Appendix*, Fig. S1*B* and normalized in *SI Appendix*, Fig. S1*C*). The best-fit parameters plotted as a function of pSpy concentration (Fig. 1*D*; error bars are the SEM from four repeats) show that A and λ (Fig. 1*D*, green and pink, respectively) are both strongly affected by preprotein concentration, while lag (Fig. 1*D*, cyan) is affected only slightly, if at all. Assuming transport takes place according to the model in Fig. 1*B* (and at least some pSpy–Pep86 is prebound), the lag should correspond to the following:

$$\text{lag} = \frac{1}{k_{\text{init}}} + \text{n}\frac{1}{k_{\text{step}}}. \qquad [1]$$

The observation that the lag is not preprotein concentration dependent is therefore expected, as none of the parameters that define it are either. The plot of λ as a function of pSpy–Pep86 concentration, meanwhile, fits fairly well to a weak binding equation (Fig. 1*D*, pink squares), giving an apparent Kd (dissociation constant, 0.57 μM) in reasonable agreement with a previously determined affinity of pSpy for SecA (0.2 μM; 26).

The fact that signal amplitude depends on preprotein concentration was surprising to us. PLs are diluted ~8,000-fold (wt/vol; i.e., weight/volume) into a reaction buffer for the transport experiment. So, for PLs with an internal 11S concentration of 40 μM (the maximum used here), at most, 5 nM preprotein needs to be imported for the transport reaction to reach completion. The external concentration of pSpy–Pep86 is therefore essentially unaffected by the transport reaction, and aside from one or another reaction component running out, there is no obvious reason for transport to stop. Thus, the reaction is reaching completion in a manner that is dependent on pSpy–Pep86 concentration but is not due to it running out—we revisit this point again below.

It should be noted that A (normalized to its maximum value within each repeat) against pSpy–Pep86 concentration produces a graph with large error bars (Fig. 1*D*, green diamonds). Presumably, these reflect the fact that A is very sensitive to multiple different experimental parameters, especially to active SecYEG and 11S concentrations in the PLs, which are highly variable between batches. To mitigate this, when possible, all subsequent comparative experiments were performed in parallel using the same batch of PLs. It should also be mentioned that when the value for λ is very low, it becomes hard to determine the *x* intercept precisely; thus, lags determined from transport reactions that reach completion quickly are more reliable.

Finally, we measured NanoLuc formation (step *iv*) in solution (no membranes present) by titrating pSpy–Pep86 against a fixed concentration of 11S. The rate of formation is approximately linear up to 4 μM (above which it becomes too fast to resolve on the plate reader) with a slope (k_{onL}) of 3.7 $\mu M^{-1} \cdot min^{-1}$ (Fig. 1*E*, orange squares). The fitted Kd for the interaction (Kd_L) is 58 ± 24 nM (Fig. 1*E*, green circles; error derived from the fit), which means that for 11S concentrations used here (generally 20 μM inside the PL and at least 5 μM), NanoLuc formation should always be completely saturated and much faster than transport (see, e.g., Fig. 1 *C* and *D* and below). Consistent with this, we have previously shown that the concentration of 11S inside the vesicles has no effect on transport kinetics of a different model substrate (proOmpA) at concentrations above 1 μM (16). Therefore, the assay reports on transport kinetics and not the formation of the active luciferase.

Determination of the Initiation and Transport Steps Using Tandem pSpys. To investigate the protein transport parameters k_{init}, k_{step}, and n, we next designed a series of four nearly identical 4× tandem pSpy–Pep86 variants ($pSpy_{4\times}$; Fig. 2*A* and *SI Appendix*, Fig. S2). In each substrate, three of the Pep86 sequences are scrambled so they retain the same aa composition but give a vastly reduced signal upon transport (*SI Appendix*, Fig. S3*A*; "D" [for "dark"] in Fig. 2*A*). The fourth is left as active Pep86 ("L"

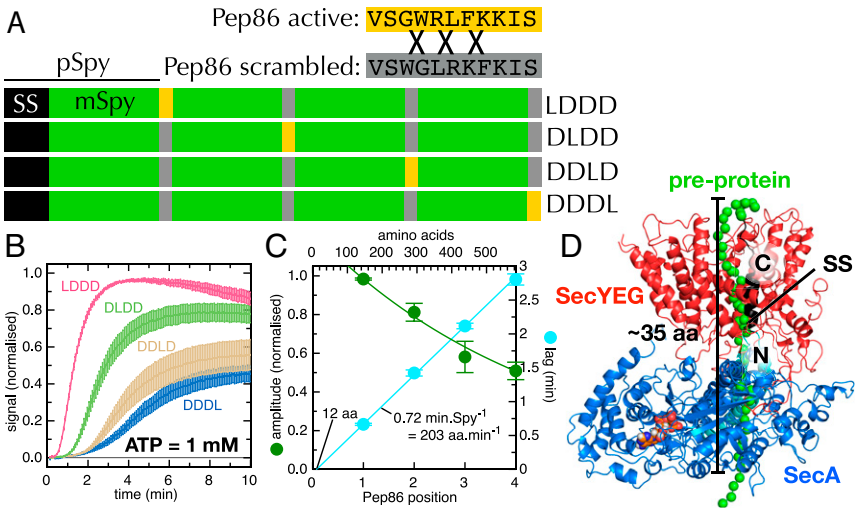

Fig. 2. The tandem pSpy–Pep86 series. (*A*) A schematic of the tandem pSpy–Pep86 series. (*B*) The average transport of 1 to 2 μM of the $pSpy_{4\times}$ series into vesicles containing 10 to 20 μM 11S, normalized to LDDD for each run. LDDD is pink, DLDD green, DDLD beige, and DDDL blue. Error bars are the SEM of eight repeats. (*C*) The normalized A (green circles) and lag (cyan circles) as a function of active Pep86 position (and equivalent in aa) for the $Spy_{4\times}$ series, extracted from the data in *B*. The fits are to straight lines (lag) and exponential decay (A). (*D*) A model of SecYEG (red) and SecA (blue) with a preprotein in the channel (SS in black and mature in green; 39). Initiation brings ~35 aa of mature domain into the SecY–SecA complex.

[for "light"] in Fig. 2*A*). Thus, the resulting proteins are identical save for the length of substrate that must be translocated before the functional Pep86 becomes accessible. This eliminates any potential differences in targeting and initiation, which we find are noticeable for short substrates (*SI Appendix*, Fig. S3 *B* and *C*). After confirming that all four bind rapidly and with high affinity to 11S (*SI Appendix*, Fig. S3 *D–G*), we carried out transport experiments initiated with saturating ATP (Fig. 2*B*). We observed that, as the position of the active Pep86 moves later (from LDDD to DDDL, Fig. 2*B*), all three parameters in the lag–exponential fit are affected in a systematic manner: the lag increases with the length of substrate before Pep86, while λ and A both decrease.

From Eq. **1**, a plot of lag as a function of n should fit to a straight line with a slope equal to the rate of transport and *y* axis intercept equal to k_{init}^{-1}. The experimental data do indeed fit well to a straight line (Fig. 2*C*, cyan line), with a slope of 0.72 min · Spy^{-1}. Because this value corresponds to n/k_{step} for a single pSpy, we cannot at this stage distinguish between many fast steps or few slow ones; however, as the mature domain of Spy (mSpy; with SS cleaved) is 146 aa long, it does allow us to determine an average transport rate of ∼200 aa per minute.

The line of best fit in Fig. 2*C* goes almost straight through the origin, which could be taken to mean that the value of $1/k_{\text{init}}$ is very small—that is, initiation is very fast compared to k_{step}. However, this does not seem consistent with previous data, which did show a slow initiation step (21). Our alternative interpretation is that initiation is accompanied by the transport of a short stretch of polypeptide, equivalent to the amount transported by k_{step}. Indeed, structural evidence suggests that the insertion of SS into the lateral gate with its N terminus facing the cytosol, a key part of initiation (1), brings about 35 aa of the mature domain into the SecY–SecA channel (Fig. 2*D*). Therefore, the simplest explanation for these results is that k_{init} (from prebound preprotein) and k_{step} (in the absence of PMF) are effectively the same process. This is consistent with the notion that the catalytic cycle of SecA is primarily regulating the opening and closing of the channel through SecY (9); the same widening event permits insertion of the SS plus 35 aa during initiation and diffusion of the preprotein during transport.

An unexpected observation from the $\text{pSpy}_{4\times}$ series is that signal amplitude also reduces as the position of the active Pep86 moves toward the C terminus (Fig. 2 *B* and *C*, green circles). This suggests that a significant proportion of in vitro transport events initiate and begin transport but do not reach completion. One simple explanation of this is that there is a chance for the translocating preprotein to become irretrievably trapped within the SecYEG complex, preventing any subsequent transport at that site (hereafter "blockage"). The rate of blockage can be estimated by fitting A as a function of Pep86 position (P) to a simple exponential decay ($A = A_0 e^{-P/\Lambda}$), where A_0 is the signal in the absence of transport failure and Λ is the average number of aa transported before blockage. The resulting fit (green line in Fig. 2*C*) is to Λ = 661 aa; in other words, during in vitro transport of $\text{pSpy}_{4\times}$, the SecYEG channel becomes irreversibly blocked after on average 3.3 min (from ∼200 aa · min^{-1}, determined above).

This also suggests that, at least for $\text{pSpy}_{4\times}$, the number of active SecYEG sites limits the reaction, not 11S—a conclusion supported by the fact that the transport signal is independent of the internal 11S concentration down to ∼5 μM (*SI Appendix*, Fig. S3 *H–J*). A likely explanation of this is that, although the concentrations of SecYEG and 11S supplied are fairly similar (see *Materials and Methods*), a large proportion of the SecYEG sites are inactive when reconstituted in vitro (27), so 11S is effectively always in excess. It has recently been shown that resetting the SecYEG translocon after a transport event is very slow compared to transport itself in vitro (28); for this reason, it is likely that we only observe a single transport event per SecYEG translocon.

The Processivity of Transport. The data shown above allow us to determine the average rate at which successful transport events occur and to estimate a rate of blockage where the channel is completely inactivated. However, it gives no information on processivity; how often does preprotein completely dissociate from the channel during transport and have to reinitiate from scratch? And does SecA dissociate and rebind during the course of a single transport reaction, as has been proposed (29–31)?

To investigate these questions, we carried out transport experiments under conditions in which multiple turnovers were prevented. When a large excess of unlabeled ("cold") $\text{pSpy}_{2\times}$ is present, it competes with pSpy–Pep86 for import sites and blocks transport of Pep86 (*SI Appendix*, Fig. S4*A*). If the excess $\text{pSpy}_{2\times}$ is instead added together with the ATP, any preformed SecYEG–SecA–preprotein complex will continue to translocate, but no new transport events can start—that is, single turnover conditions with respect to transport. This will reduce the total amplitude in two main ways: 1) by a fixed amount, as new transport events cannot start after the addition of ATP; and 2) in a length-dependent manner, from any preprotein that dissociates during transport.

When we performed this experiment using the $\text{pSpy}_{4\times}$ series, we did indeed observe both length-dependent and length-independent decreases in the signal (Fig. 3*A*, light pink versus dark pink, and *SI Appendix*, Fig. S4*B*). Fitting the quenched

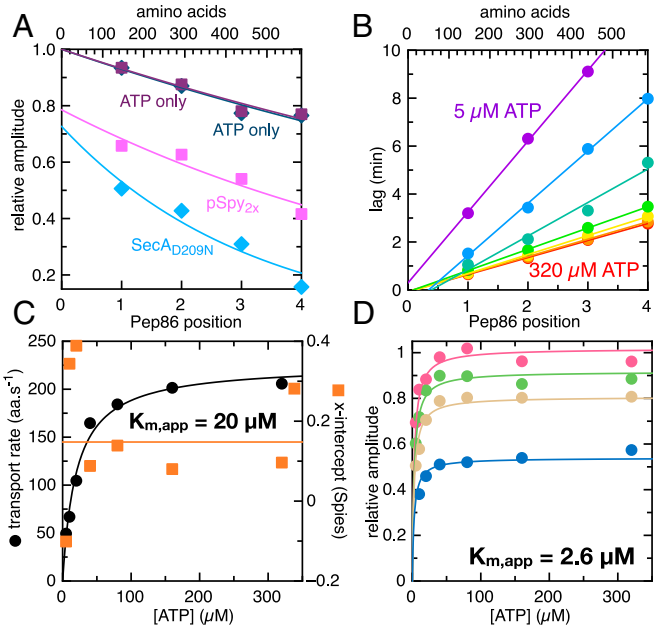

Fig. 3. Processivity and ATP dependence of transport. (*A*) The amplitude of the transport signal for tandem $\text{pSpy}_{4\times}$ series with 50 μM $\text{pSpy}_{2\times}$ (pink) or 10 μM $\text{SecA}_{\text{D209N}}$ (cyan) added at the same time as the ATP. The equivalent data with only ATP, performed in parallel, are shown in dark pink and blue, respectively (n.b., these overlay very closely, largely obscuring the blue data). The fits are to exponential decay and normalized to the fitted value of A_0 with only ATP. (*B*) Lag as a function of active Pep86 position in the $\text{Spy}_{4\times}$ series, at a range of ATP concentrations: red = 320 μM, orange = 160 μM, yellow = 80 μM, green = 40 μM, teal = 20 μM, blue = 10 μM, and purple = 5 μM. The fits are to straight lines. (*C*) The transport rate (black circles) and *x* intercept (orange squares) extracted from the fits in *B* as a function of ATP concentration. The transport is fitted to the Michaelis–Menten equation (black line), while the orange line is the mean *x* intercept. (*D*) A as a function of [ATP] for the $\text{Spy}_{4\times}$ series. The lines are global fits to a weak binding equation.

transport amplitudes to exponential decay (see above) gives Λ = 1,040 aa when excess $pSpy_{2\times}$ is added (light pink line in Fig. 3*A*) and Λ = 2,060 aa in a parallel experiment without the cold substrate (dark pink line in Fig. 3*A*). From these numbers, it appears that for transport of $pSpy_{4\times}$ into PLs, transport failure has roughly a 50% chance of permanently blocking the channel and a 50% chance of freeing the channel for another round of transport. However, as the fitting error is significant, we cannot accurately state from this how often complex dissociation occurs.

To investigate the processivity of SecA, we performed a similar experiment but using a large excess of the catalytically inactive SecA mutant $SecA_{D209N}$ (*SI Appendix*, Fig. S4*C*; 32). Because SecA is required to initiate transport, this prevents reinitiation, just as with the competing substrate, but it also prevents transport restart after SecA dissociation and rebinding. Any additional length-dependent signal decrease over and above the competing substrate is therefore indicative of multiple SecAs interacting with a single preprotein.

The results (Fig. 3*A*, light blue line; *SI Appendix*, Fig. S4*D*) give Λ = 460 aa, corresponding to a channel dwell time for SecA of 2.3 min. This is substantially lower than with a competing substrate (pink line), suggesting that one SecA can indeed be fully released from the translocating preprotein, followed by binding of another, without the preprotein being released from the channel in the interim. From this, we conclude that the number of SecAs used to transport a single substrate is determined kinetically; only one is needed, but multiples can be used if the transport takes longer than the dwell time of SecA on the machinery. An extended schematic model incorporating the additional possible fates of a translocating preprotein is shown in *SI Appendix*, Fig. S4*E*.

The ATP Dependence of Preprotein Transport. Both initiation and transport of preproteins are driven by cycles of ATP binding and hydrolysis in SecA (10). The ATP turnover reaction itself has been well characterized in the past (11, 13), but how it is coupled to transport is less well understood. We therefore measured the import of each of the $Spy_{4\times}$ series at a range of ATP concentrations; all three parameters (lag, λ, and A) are affected in a similar manner for all four substrates (Fig. 3 *B–D* and *SI Appendix*, Fig. S4*F*). As expected from Eq. **1**, the lag remains proportional to the number of Spys before the active Pep86 (and thus the number of steps n) as ATP concentration ([ATP]; and thus k_{step}) is lowered, with the slope of the line becoming steeper (Fig. 3*B*). The corresponding transport rates and *x* intercepts for these data are plotted in Fig. 3*C*. Rate as a function of [ATP] fits well to the Michaelis–Menten equation, giving an apparent K_M (Michaelis constant) for ATP of 20 μM. The *x* intercept is close to the origin and does not change significantly with [ATP] despite k_{init} also requiring ATP turnover—consistent with k_{init} simply being k_{step}. Note that as mentioned above, determining lag accurately becomes more difficult for low values of λ, hence the scatter at low [ATP].

Both A and λ versus [ATP] also fit well to the Michaelis–Menten equation for all four substrates (Fig. 3*D* and *SI Appendix*, Fig. S4*F*). The K_M for ATP determined from λ (15.4 μM, obtained by globally fitting all four data sets; *SI Appendix*, Fig. S4*F*) is very similar to that determined from lag (20 μM; Fig. 3*C*) and fairly close to the value of 46 μM determined for the ATPase activity of translocating SecA (13). The small discrepancy perhaps reflects the fact that K_M determined here only reports on successfully translocated preproteins, whereas bulk ATPase activity includes all SecA. For A (Fig. 3*D*), the apparent K_M for ATP is much lower at 2.6 μM; the discrepancy suggests that the overall amount of preprotein transported is not directly correlated with the transport rate.

Evaluating Possible Transport Models Numerically Using Berkeley Madonna. The "single exponential plus lag" equation used thus far (Fig. 1*A*) is straightforward to fit and describes each data set with reasonable accuracy; however, it is not immediately evident what λ actually corresponds to in physical terms. Furthermore, the fits deviate significantly from the data at the point where the lag and exponential meet (which we will refer to as the "start phase")—the part of the curve that should contain information about how the motor is distributed along its substrate (19). We therefore sought to fit the data more directly to physical models of transport using numerical integration techniques.

In a biochemical reaction scheme such as the one in Fig. 1*B*, the concentration of each component changes as a function of time dependent on the processes that populate it and depopulate it. Because these processes are themselves concentration dependent, the overall reaction can be described by a set of differential equations. Analytical solutions to such problems become highly complex even for fairly simple reaction schemes, so to evaluate different transport models, we used numerical integration, as implemented by the software package Berkeley Madonna. In this method, the complete set of differential equations for a given model is defined (*SI Appendix*, section S2), along with all rates and the initial concentrations of each species. Next, each concentration is recalculated in very small time increments, and the formation of the measured component—in this case, NanoLuc—is determined as a function of time. These simulated data can then be compared to experimental data, varying the unknown values to try to obtain a reasonable fit.

The model in Fig. 1*B* is defined for Berkeley Madonna in *SI Appendix*, section S2. For simplicity, two additional assumptions are made: that step *i* is at equilibrium when the reaction starts and that NanoLuc formation is instant. The first is reasonable given that the assay setup includes an 8-min incubation step prior to the addition of ATP and k_{on} is of the order of 1.25 $\mu M^{-1} \cdot min^{-1}$ (see above), while the latter is effectively true under the conditions used here (Fig. 1*E*). The value for k_{off} was set to 0.7125 min^{-1} to give $K_d = 0.57$ (as estimated from Fig. 1*D*, where $K_d = k_{off}/k_{on}$). We also include two additional rate constants: dissociation of the translocating complex, allowing reinitiation (k_{fail}); and blockage of the channel, preventing any more transport (k_{block}). This complete model is illustrated in *SI Appendix*, Fig. S5*A*. Note that the value k_{init} is also set to equal k_{step}, as per the results above; however, the same results are produced if k_{init} is set very fast and n is increased by 1. For modeling purposes, we set the concentrations of SecYEG and 11S to 4 nM and 5 nM, respectively. Although we do not know the exact concentration of active SecYEG, it makes no difference to resulting traces unless it is higher than 11S (which we know is not the case, see *SI Appendix*, Fig. S3 *H–J*).

A simulated transport curve—using reasonable values for each parameter based on the simpler fitting results above and then optimized to fit a real transport data set—is shown in Fig. 4*A*. Just as with the real data, simulated transport can be divided into four phases: a lag, characteristic of n-step sequential mechanisms; a start phase, which contains information about the number of steps and static disorder; a burst phase, produced from preformed SecYEG–SecA–preprotein complex; and an end phase, as transport slows to a halt. Note that in this model, each SecYEG only turns over a single preprotein; however, in practice, we find that allowing multiple turnovers only affects the very end of the transport curves, where it is swamped by signal decay—particularly as subsequent turnovers are likely to be significantly slower (28).

While the above model has a lot of parameters, each one only affects a limited part of the transport curve (*SI Appendix*, Fig. S5*B*). Most importantly, k_{step} and n are the only parameters that make any appreciable difference to the lag and start phases, with many fast steps giving rise to a sharp start phase and a few slow

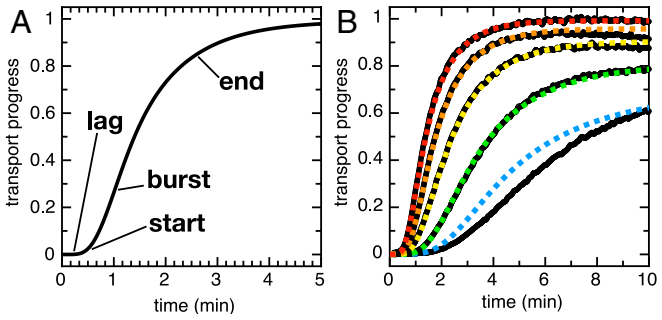

Fig. 4. A numerical modeling of transport with Berkeley-Madonna. (*A*) An example simulated transport curve for the model in *SI Appendix*, section S2.1 and Fig. S5*A*. Parameters are as follows: k_{step} = 6.3 min^{-1}; n = 6; k_{on} = 2 μM · min^{-1};k_{off} = 1.6 min^{-1}; k_{fail} = 0.19 min^{-1}; k_{block} = 0.13 min^{-1}; and brightness = 283. (*B*) The transport signal for $pSpy_{4\times}$ LDDD with 320, 40, 20, 10, and 5 μM ATP (black lines). The dotted lines are simulated data (as in *A*) with k_{step} = 6.3 min^{-1} (red), 5.05 min^{-1} (orange), 3.85 min^{-1} (yellow), 2.65 min^{-1} (green), and 1.9 min^{-1} (blue).

steps producing a more diffuse start (*SI Appendix*, Fig. S5*B*). The other parameters each affect the size of the burst phase and the shape of the end phase in a subtly different way, and we were unable to reproduce experimental data as well if any one of them was eliminated. We are therefore confident that this model represents the simplest solution that adequately describes the data. As an illustration of this, the experimental ATP concentration dependence can be reproduced down to 10 μM ATP (Fig. 4*B*) only by varying k_{step} (the only ATP-dependent rate constant).

Using the Berkeley Madonna Model to Estimate Elementary Step Size. Because the shape of the beginning of the transport curve is affected differently by n and k_{step} (and not by any other parameter), our model allows us to estimate the number of individual steps that make up transport. To do this, we fixed k_{block}, k_{on}, and k_{off} at the values approximated above and then used the Berkeley Madonna curve fit algorithm to find best fit values for k_{step}, k_{fail}, and brightness at a range of different values for n (Fig. 5*A* and *SI Appendix*, Fig. S6). The best fit is to n = 5, which equates to about one step every ∼30 aa, with a k_{step} of around 3.0 min^{-1}. The corresponding k_{fail}, 0.13 min^{-1}, is well within the expected range from the single turnover transport reaction (Fig. 3*A*).

In practice, this analysis is complicated by the phenomenon of static disorder, whereby different, ostensibly identical motors can transport at different rates (33, 34). This can lead to an underestimation of the true number of steps. For example, ensemble measurements on the helicase PcrA overestimate step size about fourfold compared to the true value determined by single-molecule analysis (33). Notwithstanding this effect, we conclude that transport is best described by a relatively small number of steps—while bearing in mind that the exact number may be an underestimate.

So what are these steps? The measured k_{cat} of the SecA ATPase activity when transporting pSpy is ∼850 min^{-1} for in vitro transport with purified components (*SI Appendix*, Fig. S7)—not too far from the previously determined value of 450 min^{-1} for proOmpA (13). This corresponds to around 610 ATP turnovers per Spy or 120 ATP turnovers per step. Clearly, therefore, each step represents many turnovers of ATP; this is also illustrated in Fig. 5*B* by the poor fitting of the data to simulations with k_{step} = 850 min^{-1} and n = 610 (i.e., where each step corresponds to a single turnover of ATP, as would be expected of a purely deterministic "power-stroke" mechanism).

In summary, each elementary transport step transports around 30 aa—or somewhat fewer, depending on static disorder—and consumes around 120 ATP molecules. The most plausible explanation for this observation is that not every ATP turnover gives rise to a transport event—that is, the ATPase activity of SecA is coupled to polypeptide movement indirectly, not directly. Indirect coupling is a hallmark of our previously proposed Brownian ratchet transport model (9, 14), wherein blockages at the entrance to the SecYEG channel trigger nucleotide exchange, giving the blockage the opportunity to diffuse through (Fig. 5*C*). In this interpretation, each step is a blockage, and the probability of any given ATP turnover resolving this blockage (p_{res}) is 0.8% (1/120) for in vitro transport of pSpy into PLs. By contrast, for a tightly coupled power-stroke motor to produce the same kinetic profile, one cycle would have to consume 120 ATP molecules (*SI Appendix*, Fig. S8)—even ignoring the fact that the proposed piston (the two-helix finger; 15) can be cross-linked in place without preventing transport (35).

Discussion

The advent of an assay capable of measuring protein transport accurately, with a time resolution of seconds, has opened the door to investigating the process on a detailed functional as well as a structural level. While well-conducted studies of the kinetics of protein transport have been performed previously (27, 36), their interpretation has always been limited by the poor time resolution inherent to end-point measurements. Using NanoLuc, we have here built up a detailed model of transport and a thorough

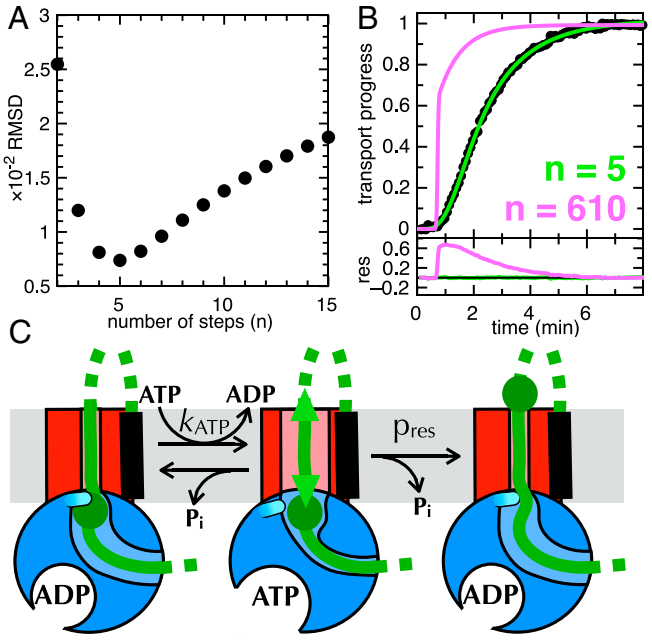

Fig. 5. The elementary transport step. (*A*) The root mean square deviation (RMSD) for the best fits to the transport data for pSpy–Pep86. In each case, k_{block} was fixed at 0.31 min^{-1} (from the green fit in Fig. 2*C*), k_{on} at 1.25 μM^{-1} · min^{-1}(from the purple versus orange data in Fig. 1*C*), and k_{off} at 0.7125 min^{-1} (to give K_d = 0.57 μM, as in Fig. 1*D*, pink fit). The fits themselves are shown in *SI Appendix*, Fig. S6. (*B*) An attempt to fit a transport model where k_{step} is the rate of ATP turnover, presented as in *SI Appendix*, Fig. S6. With many steps (n = 610 shown, chosen to give the correct lag; pink line), the start and burst phases become extremely sharp, making it impossible to fit the experimental data. The best fit trace (n = 5; green line) is shown for comparison. (*C*) A schematic of the action of ATP in the Brownian ratchet model of preprotein transport, with components colored as in Fig. 1*B*. In the ATP bound state (middle), blockages at the entrance to SecY have a probability of resolving (p_{res}) determined by their diffusion through the channel.

understanding of how each transport parameter affects the measured luminescence signal.

To analyze the data, we have developed two different approaches. Fitting to a simple model requires no specialist software and gives two useful parameters: lag, which corresponds to the minimum time required for transport; and amplitude, which correlates with the total amount of substrate transported. A complete numerical integration solution, meanwhile, validates the overall model and provides estimates for each individual rate constant. It should be noted that lag is relatively independent of experimental variables and is thus a robust measure of transport rate. It will therefore be particularly useful for evaluating differences in transport by Sec mutants, or of different preprotein substrates, with high sensitivity. Amplitude, meanwhile, is highly susceptible to experimental error and so should ideally be interpreted from experiments run in parallel using the same reagents.

Surprisingly, we find that initiation—although clearly a critical part of the mechanism for recognizing genuine Sec substrates—does not seem to contribute appreciably to the overall kinetics of transport. Indeed, if anything, the first few aa of mSpy are transported faster than the rest (Figs. 2*C* and 3*C*). A likely explanation for this is that the insertion of the SS into the lateral gate of SecA—oriented to keep the positively charged N terminus in the cytosol and bring the narrow, hydrophilic C terminus through the channel (Fig. 2*D*)—provides an extra driving force to pull the first aa across the membrane. The idea that initiation and transport are effectively the same process is further supported by a structural model of the preinitiation complex based on FRET (fluorescence resonance energy transfer) constraints, in which the SS and the beginning of the mature domain form a hairpin poised at the entrance to the channel through SecY (37).

The net transport rate of ~200 aa per minute determined here is similar to one previous estimate of transport rate for fluorescently labeled proOmpA into inverted membrane vesicles (36) but roughly 10-fold slower than translocation of unlabeled proOmpA into PLs (21). This can partly be ascribed to the nature of the substrate: proOmpA was originally chosen as a model translocation substrate precisely because it is secreted very efficiently. However, it should also be noted that the NanoLuc assay reports only on successful transport events, whereas the single-molecule assay in Fessl et al. (21) uses movement of the plug domain of SecY as a proxy for transport. Therefore, the higher rates reported in Fessl et al. (21) may also partially reflect a fraction of initiated but subsequently aborted events (represented by k_{fail} in the model in *SI Appendix*, Fig. S5*A*).

Almost all of the observed experimental data can be reproduced by the Berkeley Madonna transport model (*SI Appendix*, Fig. S5*A*) using reasonable values for each of the six rate constants. However, the strong dependence of signal amplitude on preprotein concentration (Fig. 1*D* and *SI Appendix*, Fig. S1*B*) is not explicable within this framework, as pSpy is always in huge excess, and there is nothing else to stop transport except the gradual blocking of translocons (Fig. 3*A* and *SI Appendix*, Fig. S4 *A*–*D*). A plausible explanation for this is that the Sec complex behaves like a classical membrane transporter described by Peter Mitchell (38), whereby transport is partially driven by a concentration gradient, in this case of preprotein, across the membrane; this could be either total protein or some particular feature of the translocating preprotein, such as charged residues. This is, again, a feature expected of a Brownian ratchet-style mechanism, in which transport is influenced by the relative rates of inward and outward diffusion (see *SI Appendix*, Fig. S9 for more detail), but not of a directly coupled power-stroke motor.

A slowing of transport as preprotein accumulates inside the PLs would go some way toward explaining why transport assays performed in vitro are so much slower than the rates expected in vivo (39, 40). However, it cannot explain a predicted difference of nearly 2 orders of magnitude (39, 40). A clue to this may come from the extremely low probability that any given ATP turnover event gives rise to transport in vitro ($p_{res} = 0.8\%$; see Fig. 5*C*). This value seems implausibly low, so it is very likely that other factors will increase this value substantially in vivo. These might include auxiliary drivers of transport, particularly the PMF (24, 25), and some of the many other proteins that associate with the Sec system, such as SecDF, PpiD, and YfgM (41, 42). It does, however, make sense that all these factors affect p_{res} but not ATP turnover itself; it is of course far easier to add additional driving forces to a ratchet than to a directly coupled motor.

One additional factor we believe will prove particularly critical to understanding the slow in vitro transport rates is the folding state of the preprotein, which is known to be important for enabling transport (6, 43). Chaperones generally capture preproteins in vivo as they are translated and deliver them to the membrane in an optimally translocation-competent state. In vitro, meanwhile, preproteins are diluted out of urea and so have far more opportunity to form folding intermediates that delay transport. Without extra assistance, the diffusion-based transport motor has little power to unfold preproteins; instead, it must wait for a spontaneous unfolding event prior to trapping them in an unfolded state within the channel. Moreover, it seems that some secretory proteins are delivered directly to SecA, lurking at the ribosome exit site, during their translation (44, 45). Thus, it seems plausible that in the presence of a stimulatory PMF (24), careful preprotein management, and bespoke ancillary factors, transport could easily be sped up by at least an order of magnitude.

The twin developments described here—an assay that generates high-quality transport data and a fitting process capable of describing it—together provide a fully quantitative framework for understanding the mechanism of ATP-driven transport through Sec. We anticipate that the experimental and data analysis approaches will be very useful in the future, both for furthering our understanding of the bacterial Sec machinery and also, far more broadly, for studying many other membrane transport processes.

Materials and Methods

Reagents. All previously reported reagents for transport assays, including SecYEG, SecA, pSpy, and PLs, were produced exactly as described previously (16). PLs containing only SecYEG for ATPase assays were prepared as described in ref. 11. The $pSpy_{2\times}$ gene was synthesized commercially (GeneArt Gene Synthesis service, Thermo Fisher Scientific) and then cloned into the plasmid vector pBAD/*myc*-His C and expressed exactly as pSpy–Pep86 (16).

The $Spy_{4\times}$ series was constructed by first ordering three fragments of Spy containing two tandem repeats of the mature region, each with a different combination of "light" (L, active Pep86, VSGWRLFKKIS) or "dark" (D, inactive pep86, VSWGLRKFKIS) Pep86 sequences in the following combinations: DD, LD, and DL, where, for example, DD contained two inactive HiBiT sequences at the C terminus of each mature region of Spy (produced by the GeneArt Gene Synthesis service). For cloning purposes, each fragment began with residue A24 of pSpy and ended with a GSG linker immediately following the second Pep86 sequence (sequence 1 in *SI Appendix*, Fig. S2). The fragment was cloned into pBAD-pSpy-V5-pep86-TEV-His (16; sequence 2 in *SI Appendix*, Fig. S2) using site-directed ligase-independent mutagenesis (46). More specifically, the fragments were cloned in the place of Spy–V5, using the same primers to introduce a ZraI site (GACGTC) immediately after the fragment and before the TEV cleavage site of the template, to give pBAD-(LL, LD, or DL)-ZraI-TEV-His (sequence 3 in *SI Appendix*, Fig. S2). The synthesized fragments were then amplified using linear PCR and cloned into the ZraI site of pSpy LL, LD, and DL to give DDDD, LDDD, DLDD, DDLD, and DDDL (sequence 4 in *SI Appendix*, Fig. S2).

NanoLuc Formation Assays. NanoLuc formation was measured at 25 °C in a BioTek Synergy Neo2 plate reader. A dilution series of pSpy–Pep86 was prepared in the wells using TKM (20 mM Tris-HCl pH 8.0, 50 mM KCl, 2 mM $MgCl_2$) with furimazine (to 1/500) and Prionex (to 0.125%), with a volume of 100 μl per well. The reactions were started by injecting 25 μl 11S at 1 nM in TKM (to give 200 pM final) and then shaken for 2 s, and the luminescence was monitored with no emission filter.

NanoLuc Transport Experiments. Standard transport experiments were performed at 25 °C, exactly as in our recent methods paper (16). Essentially, master mixes were assembled containing all transport components except preprotein and ATP (unless otherwise stated). Unless otherwise specified, we used PLs with an internal 11S concentration of 20 μM, resuspended approximately sevenfold (wt/vol) to give a final concentration of 9.2 μM SecYEG (of which half ∼4.6 μM is oriented correctly to participate in transport; see ref. 9). These were then diluted 550-fold into a reaction buffer, giving SecYEG ∼8.4 nM and 11S ∼5.2 nM. Note, however, that a large fraction of the SecYEG translocons are expected to be inactive (27), and empirically, we observe that 11S is in excess over active SecYEG translocons even at 5 μM internal concentration (equivalent to 1.3 nM total; see *SI Appendix*, Fig. S3 *H–J*). SecA and pSpy were generally provided at 1 μM, unless otherwise specified.

To follow transport, we first added preprotein and measured background for 8 min. Transport itself was then initiated by the addition of ATP (to 1 mM unless otherwise stated) and then monitored for 25 min or until all reactions had reached completion. In most cases, eight reactions were performed in parallel, and luminescence was measured using a BioTek Synergy Neo2 plate reader. These luminescence values reflect the rate of photon emission, which is generally proportional to NanoLuc concentration over the measured time ranges (16). For the earlier reactions with different initiation conditions (Fig. 1*C*), reactions were instead performed one at a time in a Jobin Yvon Fluorolog (Horiba) with the lamp turned off.

For subsequent reactions in which additional reagents were added together with the ATP (Fig. 3 *A* and *B*), we modified the plate reader protocol to allow manual injection. Reactions of 100 μl with all components at 1.2× final concentration were assembled as above (except with SecA at 100 nM final instead of 1 μM) and measured for 8 min after the addition of preprotein. The plate was then ejected, and 20 μl ATP together with the other reagent—both at 6× final concentration—were added and mixed immediately using a multichannel pipette. Measurement was then resumed as fast as possible. The manual mixing step adds an additional constant error to reaction time, which we estimate to be less than 5 s.

Data Analysis. Initial data processing was performed using pro Fit 7 (Quansoft). Raw data before the addition of ATP were fitted to the single exponential plus lag model (*SI Appendix*, section S1.1), and the fits (background) were subtracted to give the transport signal (*SI Appendix*, Fig. S1*A*). Corrected data were then fitted to the same model to give lag, λ, and A for transport.

The model for Berkeley Madonna is described in detail in *SI Appendix*, section S2.

ATPase Assays. Steady-state ATPase assays were performed as in ref. 11, with ATP consumption calculated from the decrease in NADH (reduced nicotinamide adenine dinucleotide) absorbance at 340 nm and measured in a Lambda 25 spectrophotometer (PerkinElmer). The reactions were conducted in a TKM buffer with final concentrations as follows: 230 nM SecYEG in PLs, 60 nM SecA, 2 mM phosphoenol pyruvate, 6 to 10 units of pyruvate kinase and 9 to 14 units of lactate dehydrogenase (Merck), 0.2 mM NADH, pSpy at a specified concentration, and 1 mM ATP. The reactions were incubated at 25 °C for 5 min prior to the addition of ATP or pSpy, and then ATP was added and the basal SecA ATPase rate measured for 10 min. Finally, the translocation ATPase rate was measured following the addition of pSpy. The ATPase rates were calculated from the slope of the line as in ref. 11.

Data Availability. All study data are included in the article and supporting information.

ACKNOWLEDGMENTS. This work was funded by the Biotechnology and Biological Sciences Research Council (BB/S008349/1 and BB/N015126/1 to D.W.W. and I.C.) and the Wellcome Trust (104632 to W.J.A. and I.C.). We thank Robin Corey for critical reading of the manuscript.

1. B. Van den Berg *et al.*, X-ray structure of a protein-conducting channel. *Nature* **427**, 36–44 (2004).
2. J. F. Hunt *et al.*, Nucleotide control of interdomain interactions in the conformational reaction cycle of SecA. *Science* **297**, 2018–2026 (2002).
3. J. Zimmer, Y. Nam, T. A. Rapoport, Structure of a complex of the ATPase SecA and the protein-translocation channel. *Nature* **455**, 936–943 (2008).
4. B. W. Bauer, T. A. Rapoport, Mapping polypeptide interactions of the SecA ATPase during translocation. *Proc. Natl. Acad. Sci. U.S.A.* **106**, 20800–20805 (2009).
5. K. S. Cannon, E. Or, W. M. Clemons Jr, Y. Shibata, T. A. Rapoport, Disulfide bridge formation between SecY and a translocating polypeptide localizes the translocation pore to the center of SecY. *J. Cell Biol.* **169**, 219–225 (2005).
6. R. A. Corey *et al.*, ATP-induced asymmetric pre-protein folding as a driver of protein translocation through the Sec machinery. *eLife* **8**, e41803 (2019).
7. V. A. M. Gold, S. Whitehouse, A. Robson, I. Collinson, The dynamic action of SecA during the initiation of protein translocation. *Biochem. J.* **449**, 695–705 (2013).
8. L. Li *et al.*, Crystal structure of a substrate-engaged SecY protein-translocation channel. *Nature* **531**, 395–399 (2016).
9. W. J. Allen *et al.*, Two-way communication between SecY and SecA suggests a Brownian ratchet mechanism for protein translocation. *eLife* **5**, e15598 (2016).
10. A. Economou, J. A. Pogliano, J. Beckwith, D. B. Oliver, W. Wickner, SecA membrane cycling at SecYEG is driven by distinct ATP binding and hydrolysis events and is regulated by SecD and SecF. *Cell* **83**, 1171–1181 (1995).
11. V. A. M. Gold, A. Robson, A. R. Clarke, I. Collinson, Allosteric regulation of SecA: Magnesium-mediated control of conformation and activity. *J. Biol. Chem.* **282**, 17424–17432 (2007).
12. R. Lill *et al.*, SecA protein hydrolyzes ATP and is an essential component of the protein translocation ATPase of Escherichia coli. *EMBO J.* **8**, 961–966 (1989).
13. A. Robson, V. A. M. Gold, S. Hodson, A. R. Clarke, I. Collinson, Energy transduction in protein transport and the ATP hydrolytic cycle of SecA. *Proc. Natl. Acad. Sci. U.S.A.* **106**, 5111–5116 (2009).
14. Z. Ahdash *et al.*, HDX-MS reveals nucleotide-dependent, anti-correlated opening and closure of SecA and SecY channels of the bacterial translocon. *eLife* **8**, E1786 (2019).
15. B. W. Bauer, T. Shemesh, Y. Chen, T. A. Rapoport, A "push and slide" mechanism allows sequence-insensitive translocation of secretory proteins by the SecA ATPase. *Cell* **157**, 1416–1429 (2014).
16. G. C. Pereira *et al.*, A high-resolution luminescent assay for rapid and continuous monitoring of protein translocation across biological membranes. *J. Mol. Biol.* **431**, 1689–1699 (2019).
17. A. L. Lucius, N. K. Maluf, C. J. Fischer, T. M. Lohman, General methods for analysis of sequential "n-step" kinetic mechanisms: Application to single turnover kinetics of helicase-catalyzed DNA unwinding. *Biophys. J.* **85**, 2224–2239 (2003).
18. J. A. Ali, T. M. Lohman, Kinetic measurement of the step size of DNA unwinding by Escherichia coli UvrD helicase. *Science* **275**, 377–380 (1997).
19. S. E. McClelland, D. T. F. Dryden, M. D. Szczelkun, Continuous assays for DNA translocation using fluorescent triplex dissociation: Application to type I restriction endonucleases. *J. Mol. Biol.* **348**, 895–915 (2005).
20. R. A. Corey *et al.*, Unlocking the bacterial SecY translocon. *Structure* **24**, 518–527 (2016).
21. T. Fessl *et al.*, Dynamic action of the Sec machinery during initiation, protein translocation and termination. *eLife* **7**, e35112 (2018).
22. G. Gouridis, S. Karamanou, I. Gelis, C. G. Kalodimos, A. Economou, Signal peptides are allosteric activators of the protein translocase. *Nature* **462**, 363–367 (2009).
23. D. Hizlan *et al.*, Structure of the SecY complex unlocked by a preprotein mimic. *Cell Rep.* **1**, 21–28 (2012).
24. L. Brundage, J. P. Hendrick, E. Schiebel, A. J. Driessen, W. Wickner, The purified E. coli integral membrane protein SecY/E is sufficient for reconstitution of SecA-dependent precursor protein translocation. *Cell* **62**, 649–657 (1990).
25. E. Schiebel, A. J. Driessen, F. U. Hartl, W. Wickner, Delta mu H+ and ATP function at different steps of the catalytic cycle of preprotein translocase. *Cell* **64**, 927–939 (1991).
26. K. E. Chatzi *et al.*, Preprotein mature domains contain translocase targeting signals that are essential for secretion. *J. Cell Biol.* **216**, 1357–1369 (2017).
27. P. Bariya, L. L. Randall, Coassembly of SecYEG and SecA fully restores the properties of the native translocon. *J. Bacteriol.* **201**, JB.00493-18 (2018).
28. C. Mao, P. Bariya, Y. Suo, L. L. Randall, Comparison of single and multiple turnovers of SecYEG in *E. coli*. *J. Bacteriol.*, 10.1128/jb.00462-20 (2020).
29. C. Mao *et al.*, Stoichiometry of SecYEG in the active translocase of Escherichia coli varies with precursor species. *Proc. Natl. Acad. Sci. U.S.A.* **110**, 11815–11820 (2013).
30. J. Young, F. Duong, Investigating the stability of the SecA-SecYEG complex during protein translocation across the bacterial membrane. *J. Biol. Chem.* **294**, 3577–3587 (2019).
31. K. Morita, H. Tokuda, K. Nishiyama, Multiple SecA molecules drive protein translocation across a single translocon with SecG inversion. *J. Biol. Chem.* **287**, 455–464 (2012).
32. A. Robson, A. E. G. Booth, V. A. M. Gold, A. R. Clarke, I. Collinson, A large conformational change couples the ATP binding site of SecA to the SecY protein channel. *J. Mol. Biol.* **374**, 965–976 (2007).
33. J. Park *et al.*, PcrA helicase dismantles RecA filaments by reeling in DNA in uniform steps. *Cell* **142**, 544–555 (2010).
34. P. R. Bianco *et al.*, Processive translocation and DNA unwinding by individual RecBCD enzyme molecules. *Nature* **409**, 374–378 (2001).

35. S. Whitehouse *et al*., Mobility of the SecA 2-helix-finger is not essential for polypeptide translocation via the SecYEG complex. *J. Cell Biol.* **199**, 919–929 (2012).
36. D. Tomkiewicz, N. Nouwen, R. van Leeuwen, S. Tans, A. J. M. Driessen, SecA supports a constant rate of preprotein translocation. *J. Biol. Chem.* **281**, 15709–15713 (2006).
37. Q. Zhang, Y. Li, R. Olson, I. Mukerji, D. Oliver, Conserved SecA signal peptide-binding site revealed by engineered protein chimeras and förster resonance energy transfer. *Biochemistry* **55**, 1291–1300 (2016).
38. P. Mitchell, A general theory of membrane transport from studies of bacteria. *Nature* **180**, 134–136 (1957).
39. I. Collinson, R. A. Corey, W. J. Allen, Channel crossing: How are proteins shipped across the bacterial plasma membrane? *Philos. Trans. R. Soc. Lond. B Biol. Sci.* **370**, 20150025 (2015).
40. T. Cranford-Smith, D. Huber, The way is the goal: How SecA transports proteins across the cytoplasmic membrane in bacteria. *FEMS Microbiol. Lett.* **365**, fny093 (2018).
41. J. A. Pogliano, J. Beckwith, SecD and SecF facilitate protein export in Escherichia coli. *EMBO J.* **13**, 554–561 (1994).
42. B. Jauss *et al*., Noncompetitive binding of PpiD and YidC to the SecYEG translocon expands the global view on the SecYEG interactome in *Escherichia coli*. *J. Biol. Chem.* **294**, 19167–19183 (2019).
43. A. Tsirigotaki *et al*., Long-lived folding intermediates predominate the targeting-competent secretome. *Structure* **26**, 695–707.e5 (2018).
44. D. Huber *et al*., SecA cotranslationally interacts with nascent substrate proteins in vivo. *J. Bacteriol.* **199**, e00622-e16 (2016).
45. R. Singh *et al*., Cryo-electron microscopic structure of SecA protein bound to the 70S ribosome. *J. Biol. Chem.* **289**, 7190–7199 (2014).
46. J. Chiu, P. E. March, R. Lee, D. Tillett, Site-directed, ligase-independent mutagenesis (SLIM): A single-tube methodology approaching 100% efficiency in 4 h. *Nucleic Acids Res.* **32**, e174 (2004).